Available online at www.sciencedirect.com

ScienceDirect

Geochimica et Cosmochimica Acta 266 (2019) 292–306

Geochimica et Cosmochimica Acta

www.elsevier.com/locate/gca

Diffusion-controlled and concentric growth zoning revealed by phosphorous in olivine from rapidly ascending kimberlite magma, Benfontein, South Africa

Geoffrey H. Howarth [a,*], Juliane Gross [b]

[a] Department of Geological Sciences, University of Cape Town, Rondebosch 7701, South Africa
[b] Department of Earth and Planetary Sciences, Rutgers University, 610 Taylor Road, Piscataway, NJ 08854, USA

Received 8 April 2019; accepted in revised form 3 August 2019; available online 10 August 2019

Abstract

Olivine chemistry has been widely used to track the petrogenesis of mafic and ultramafic magmas from their mantle source to eruption at the surface. A major challenge in these studies is deciphering crystal growth versus diffusion controlled zoning. Here we report a multi-element approach using high-precision electron microprobe techniques to evaluate crystal growth versus diffusion in kimberlitic olivine from the Benfontein kimberlite, South Africa. These results have implications for both the petrogenesis of kimberlite magmas and the understanding of crystal growth and diffusion-based zoning in igneous olivine in general.

The Benfontein olivine contain multiple phosphorous (P)-rich and P-poor zones. Core zones are characterized by homogenous low-P (<78 ppm) concentrations, consistent with xenocrystic origins. Gradational changes in Fo, Ni, Cr and other minor/-trace elements at core-margins are similarly characterized by constant low-P concentrations that are indistinguishable from the central regions of the core. Olivine P-maps effectively outline the original xenocryst core, whereas gradational margins are interpreted as diffusion controlled zones related to early-stage equilibration of xenocrystic olivine with proto-/kimberlite melt.

Multiple P-poor (100–150 ppm) and P-rich (200–450 ppm) concentric, oscillatory zones with inclusions of kimberlitic oxide phases are observed surrounding the low-P xenocrystic cores. Oxide phases change from chromite in the inner zones to ilmenite in the intermediate zones to magnetite-rich spinel in the outer zones of the olivine. The P-zoning corresponds with changes in Fo content implying that stages of crystal growth was preserved by both fast and slow diffusing elements rather than diffusion processes. Elements compatible with olivine (±chromite) crystallization (i.e., Ni and Cr) display a constant decrease across all zones, suggesting that magma mixing is unlikely a controlling process for P-zoning. We interpret P-rich zones to result from stages of solute trapping related of rapid disequilibrium growth driven by extrinsic factors such as changes in pressure-temperature during kimberlite evolution. In contrast, P-poor zones represent stages of equilibrium crystal growth. The outer olivine zones are characterized by an increase in Fo contents up to Fo_{96}, and in conjunction with a change to more Fe^{3+}-rich oxides, suggest late stage increase in fO_2.

Correlated Fo and P changes in the Benfontein olivine suggest that major element zonation represents an example where crystal growth-induced Fo zoning has been preserved in olivine. Furthermore, P-rich olivine zones preserve evidence for concentric growth rather than common dendritic structures seen in other occurrences. These results have implications for understanding the effect of magma dynamics and changes in pressure-temperature-fO_2 conditions on olivine growth in igneous rocks.

Keywords: Olivine; Phosphorous; Concentric growth; Diffusion; Magma mixing; Kimberlite

* Corresponding author.
E-mail address: geoffrey.howarth@uct.ac.za (G.H. Howarth).

https://doi.org/10.1016/j.gca.2019.08.006
0016-7037/

1. INTRODUCTION

Olivine is an extremely valuable petrological tool as its chemistry can be used to decipher magma petrogenesis and to infer mantle source rock lithology (e.g., Sobolev et al., 2007; Foley et al., 2013; Herzberg et al., 2016; Howarth and Harris, 2017; Gordeychik et al., 2018). Diffusion profiles in olivine can also be used to constrain timescales for magma residence and eruption in crustal chambers (e.g., Costa and Chakraborty, 2004; Costa et al., 2008). Using olivine to constrain magma petrogenesis and source rock lithology relies on the assumption that olivine chemistry is a function of crystal growth whereas diffusion profile modelling assumes that olivine chemical zoning is related to equilibration or diffusion-based formation. Understanding crystal growth versus diffusion zoning in olivine, however, is no trivial task. The rates of chemical diffusion for different elements in olivine vary significantly, from those that diffuse relatively quickly (e.g., Fe-Mg; timescale of days to years for 5–300 μm scale grain) to those that diffuse slowly (e.g., Al and Cr; timescale of days to hundreds of years for 5–300 μm scale grain) and those that are almost immobile (e.g., P; years to thousands of years for 5–300 μm scale grain) (timescales as summarised by Lynn et al., 2018 and references therein). Phosphorous zoning in olivine has recently attracted attention due to its near-immobile nature in olivine and commonly preserves crystal growth features that are not seen in other elements (e.g., Milman-Barris et al., 2008; Tschegg et al., 2010; Sakyi et al., 2012; Gross et al., 2013; Shearer et al., 2013; Elardo and Shearer, 2014; Welsch et al., 2014; Shea et al., 2015; McCanta et al., 2016; Baziotis et al., 2017; Manzini et al., 2017; Xing et al., 2017; Ersoy et al., 2019; Watson et al. (2015)). This has led to debate over crystal growth versus diffusion-based zoning of Fe-Mg as well as minor elements such as Ni, Cr, and Al in olivine. Shea et al. (2015) suggested that growth induced chemical zoning of fast diffusing elements, such as Fe-Mg, may seldom be preserved. Milman-Barris et al. (2008) as well as numerous other studies listed above have found that P enriched zones do not correspond with changes in Fo contents in experimental or natural sample investigations. Thus, robust evidence for growth induced major element zoning in olivine is required and the best way to achieve this would be through multi-element zoning studies where correlation between fast and slow diffusing elements can be observed.

Kimberlite magmas are composed of abundant (~50 vol.%) and complex olivine populations ranging in size from megacrysts (>1 cm), to macrocrysts (>0.5 mm), and to microcrysts (<0.5 mm) (e.g., Clement and Skinner, 1984; Mitchell, 2008). Kimberlites are commonly divided based on texture where macrocrystic kimberlites retain their olivine population *en route* to the surface while aphanitic kimberlites are generally interpreted to have fractionated the coarser grained olivines at some stage *en route* to the surface (e.g., Mitchell, 2008; Howarth et al., 2011). Kimberlite magmas ascend from the mantle to the surface on the order of hours to days (e.g., Kelley and Wartho, 2000; Peslier et al., 2008) and should retain primary olivine chemistry with little time for subsequent diffusion with the host melt. Thus, such olivine grains are excellent candidates to observe olivine growth features rather than diffusion related zoning. Complex internal zoning in kimberlitic olivine has been identified in olivine associated with fresh kimberlites worldwide (e.g., Fedortchouk and Canil, 2004; Kamenetsky et al., 2007; Arndt et al., 2010; Pilbeam et al., 2013; Bussweiler et al., 2015; Cordier et al., 2015; Sobolev et al., 2015; Howarth and Taylor, 2016; Moore and Costin, 2016; Giuliani et al., 2017; Lim et al., 2018; Giuliani, 2018; Sobolev et al., 2018). Olivine cores are generally interpreted to represent mantle xenocrysts, however, much debate revolves around a diffusive versus crystal growth origin for gradational or transitional chemical zones between xenocrystic cores and surrounding zones (e.g., Pilbeam et al., 2013; Cordier et al., 2015; Howarth and Taylor, 2016; Giuliani and Foley, 2016; Moore, 2017). Howarth and Taylor (2016) previously showed that the core-margin zones for the Benfontein olivine were enriched in Cr and other trace elements relative to the cores and other surrounding zones. They interpreted these Cr-rich core-margin zones to be related to early stage equilibration with a proto-kimberlite melt in the lithospheric mantle. Other previous studies of olivine in kimberlites from Greenland have interpreted 'transitional' olivine zones at the contact between cores and margins to result from an early stage of metasomatism in the lithospheric mantle during orthopyroxene assimilation preceding the ascent of the kimberlite magma to the surface (e.g., Cordier et al., 2015). However, such an interpretation has been met with opposition where other researchers suggest such transitional zones represent early liquidus olivine that crystallized after orthopyroxene assimilation during ascent to the surface (e.g., Giuliani and Foley, 2016) and can be explained by fractional crystallization using a specific set of appropriate partition coefficients (e.g., Moore, 2017). These complex internal xenocryst cores and transitional zones in kimberlitic olivine are generally surrounded by zones of olivine that was on the liquidus at that specific time. This "liquidus olivine" is characterized by decreasing Ni concentrations buffered at constant Fo contents and typically contains chromite inclusions (e.g., Giuliani, 2018). Subsequent fine rinds of high-Fo (>90) olivine form the outer zones of these complex kimberlite olivine grains (see Giuliani, 2018 for a review on olivine in kimberlites for detailed discussion). Ultimately, kimberlitic olivine tracks multiple stages of petrogenesis from early stages of metasomatism, subsequent olivine fractionation, and changes in fO_2 conditions related to extremely high olivine Fo contents (up to Fo_{98}) (reviewed by Giuliani, 2018).

The objectives of the current study are: (1) to explore the use of phosphorous zoning in kimberlitic olivine to resolve the conundrum of diffusion vs. crystal growth zones and (2) observe the features of primary growth induced zoning of olivine. Here we report the discovery of concentric phosphorous zoning in olivine macrocrysts from the Benfontein kimberlite, South Africa, that corresponds with changes in Fo contents as well as other minor elements (e.g., Ni) and trace elements (e.g., Ti, Cr). The results of this study place constraints on understanding the complex nature of kimberlite petrogenesis as well as understanding P-zoning of

igneous olivine for the use in distinguishing diffusion versus crystal growth in olivine-bearing magma systems. In addition, we present robust evidence for the concentric growth of olivine rather than common dendritic-type growth observed in many other igneous rocks.

2. HIGH-PRECISION ELECTRON MICROPROBE (EPMA) TECHNIQUES

Quantitative electron probe microanalyses (EPMA) of olivine were performed using the JEOL JXA-8200 Superprobe at Rutgers University (RU) in the department of Earth and Planetary Sciences. Olivine grains were analyzed for Si, Mg, Fe, P, Ca, Ti, Cr, Co, Ni, Zn, Mn, and Al using an acceleration voltage of 15 kV, a beam current of 200 nA, and a focused 1-micron beam. Peak counting times were calculated following the method by Sobolev et al. (2007) and were: 20 s for Si, Fe, and Mg; 180 s for P, Ca, Ti, Cr, Co, and Ni; and 240 s for Zn, Al, and Mn. The Probe for Windows MAN protocol was used for background measurements (Donovan, 2012) and the standard ZAF correction was applied to the data. San Carlos olivine standard was analyzed at regular intervals throughout every run session to correct for potential drift. Analytical standards were well characterized natural and synthetic oxides and minerals including: olivine (Si, Mg), fayalite (Fe), Mn-olivine (Mn), Co-olivine (Co), Ni-olivine (Ni), corundum (Al), chromite (Cr), apatite (P), diopside (Ca), rutile (Ti), Zn-oxide (Zn). Data quality was ensured by analyzing secondary standards as unknowns. Detection limits at 3σ (99 % confidence level) and errors (1σ) were obtained from the Probe for Windows program (Donovan, 2012). Average detection limits (in wt.%) are: 0.018 for FeO; 0.017 for ZnO; 0.005 for MnO; 0.006 for SiO_2; 0.004 for MgO; 0.002 for Cr_2O_3, P_2O_5, and Al_2O_3; 0.003 for CoO and NiO; and 0.001 for CaO and TiO_2. The average analytical errors of Si, Mg and Fe are ~0.08%, ~0.08% and ~0.59% respectively. Average analytical errors for trace elements Ni, Mn, Ca, Cr, Zn, Co, P, Ti, and Al are 21 ppm, 40 ppm, 7 ppm, 15 ppm, 122 ppm, 17 ppm, 16 ppm, 10 ppm, and 10 ppm, respectively. Oxide totals were less then ±1% of 100%. Chemical formulae were calculated for all analyses, and only data were accepted with T-sites having 1.01–0.99 cations and M-sites having 2.02–1.98 cations when normalized to four oxygens to ensure high data quality.

Backscattered electron images and qualitative elemental X-ray maps of the olivine were taken simultaneously using the JEOL JXA-8200 Superprobe at RU with an accelerating voltage of 15 kV, beam current of 300nA, pixel dwell times between 450 ms and 700 ms, and a step size between 1 and 2 μm depending on the size of the olivine grains. Wavelength dispersive spectrometers (WDS) were used to map for P, Cr, and Ni, with P kα measured on three spectrometers simultaneously; Si, Mg, Fe, and Mn were mapped using the energy dispersive spectrometer (EDS).

3. RESULTS

The sample analyzed in this study is from the John Gurney mantle collection housed at the University of Cape Town, South Africa. Kimberlites commonly undergo late-stage deuteric alteration resulting in olivine being completely serpentinized, however, the sample JJG-2241 analyzed in this study is a rare example of an ultra-fresh macrocrystic kimberlite (i.e., fresh olivine with minor serpentine alteration), as previously described by Howarth and Taylor (2016). Four representative olivine macrocrysts were selected for detailed high-precision EPMA mapping and quantitative spot analyses (Figs. 1 and 2). All data is presented in the online appendix.

The analyzed olivine can be separated into two types based on their zoning patterns, consistent with previous interpretations of Howarth and Taylor (2016): (a) Olivine 1 and 3 that are characterized by the presence of P-rich zones, hereafter termed type I olivine (Fig. 1); and (b) Olivine 2 and 4 that do not contain P-rich zones, hereafter termed type II olivine (Fig. 2). Type I olivine grains are subdivided into six zones based on major and trace element concentrations: (1) cores (100–250 μm), (2) core-margin (10–100 μm), (2a) internal rim (10–20 μm), (3) main rim (20–150 μm), (4) type I (T1) rim (20–100 μm), and (5) rind (20–25 μm) (Fig. 3). The type II olivine can be sub-divided into five zones: (1) core (250–400 μm), (2) core-margin (20–150 μm), (2a) internal rim (~5 μm), (3) main rim (35–200 μm), and (4) type II (T2) rim (25–50 μm) (Fig. 3). The main difference between the type I and II olivine grains is the absence of P-rich T1 rims and the presence of the Ti-rich T2 rims in the type II olivine. Each of these zones from core to outer rind are described in sequence for both type I and II olivine below (Figs. 1 and 2). Olivine commonly contain more than one core (Fig. 1e), which represent overgrowth of polycrystalline xenocrystic mantle olivine, as previously shown by Howarth and Taylor (2016).

Oxide phases are observed as chadacrysts in the olivine grains and display variation in chemistry related to their location within the grains (Figs. 1 and 2). In the type I olivine, chromite grains are observed within the main rim zone whereas ilmenite is observed in the T1 (P-rich) zones, and magnetite-rich spinel at the outer rims (Fig. 1). For type II olivine, ilmenite is a rare chadacryst phase and is generally only observed within cracks/fractures whereas chromite is common in the main rim zone (Fig. 2). The oxide relationships were observed throughout the thin section in multiple grains and is not restricted to the four grains analyzed in detail.

3.1. Core and core-margin chemistry

The core chemistry of individual grains in both the type I and II olivine analyzed in this study is homogeneous with no zoning noted in the major and trace elements analyzed. The type I cores have lower Fo contents ($Fo_{88.9\text{-}89.5}$) whereas the type II olivine analyzed are more Mg-rich ($Fo_{92.6}$). The type I and II cores are also characterized by differences in minor and trace element concentrations. The type I cores have higher Ni (2808–2854 ppm), Ca (625–660 ppm), Mn (850–924 ppm), and Al (141–243 ppm) relative to the type II with lower Ni (2568–2616 ppm), lower Ca (255–285 ppm), lower Mn (703–771 ppm), and lower Al (75–86 ppm).

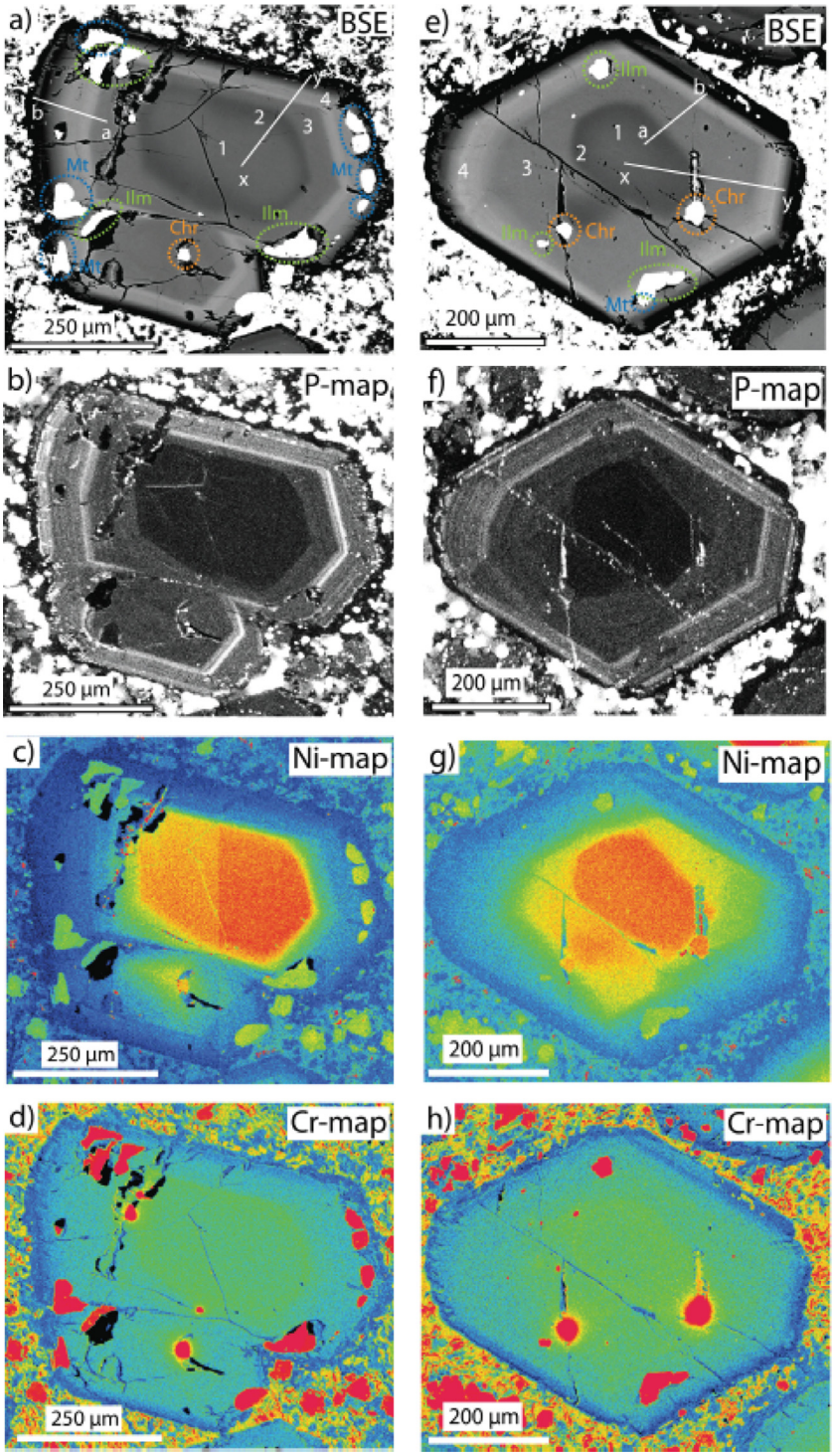

Fig. 1. Backscatter electron (BSE) images and EPMA phosphorous, nickel, and chromium maps (i.e., P-maps) for type I Benfontein kimberlite olivine. (a)–(d) olivine 3 and (e)–(h) olivine 1. In the P-maps, the brighter colours (i.e., white) represent higher P concentrations. In Ni and Cr maps, hotter colours (i.e., red/orange) represent higher concentrations of trace elements relative to colder colours (i.e., blue). The x-y and a-b solid lines indicate the location of EPMA spot traverses. Zones 1–4 represent: (1) Cores, (2) core-margin, (3) main rim, and (4) T1 rim. The internal rims described in the text are located between 2 and 3. Chr – chromite; Ilm – ilmenite; Mt – Ti-magnetite. (For interpretation of the references to colour in this figure legend, the reader is referred to the web version of this article.)

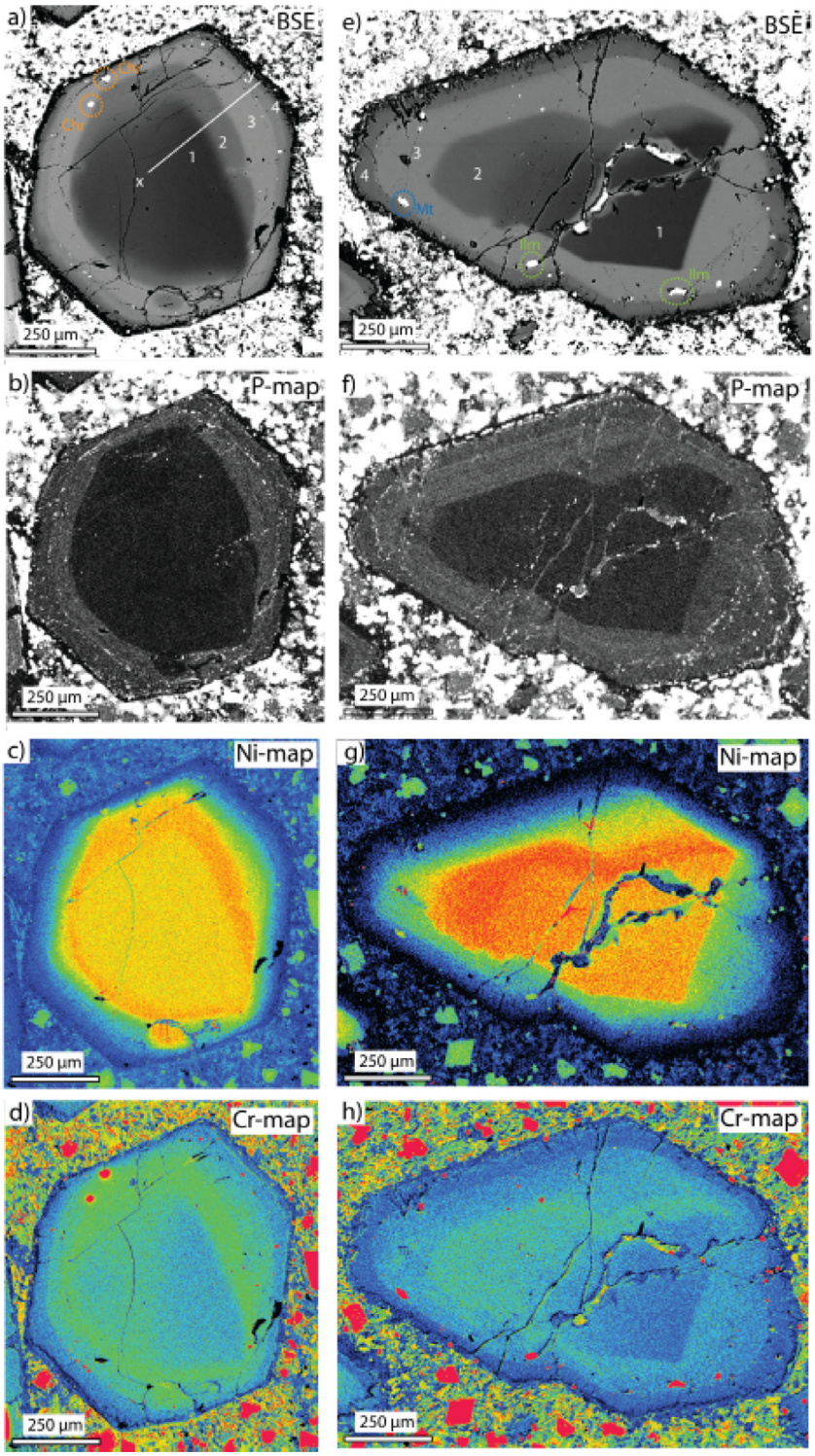

Fig. 2. Backscatter electron (BSE) images and EPMA phosphorous, nickel, and chromium maps (i.e., P-maps) for type II Benfontein kimberlite olivine. (a)–(d) olivine 4 and (e)–(h) olivine 2. In the P-maps, the brighter colours (i.e., white) represent higher P concentrations. In Ni and Cr maps, hotter colours (i.e., red/orange) represent higher concentrations of trace elements relative to colder colours (i.e., blue). The x-y solid line indicates the position of EPMA spot analysis traverse. Zones 1–4 represent: (1) core, (2) core-margin, (3) main rim, and (4) T2 rim. The internal rim is located between 2 and 3. Chr – chromite; Ilm – ilmenite; Mt – Ti-magnetite. (For interpretation of the references to colour in this figure legend, the reader is referred to the web version of this article.)

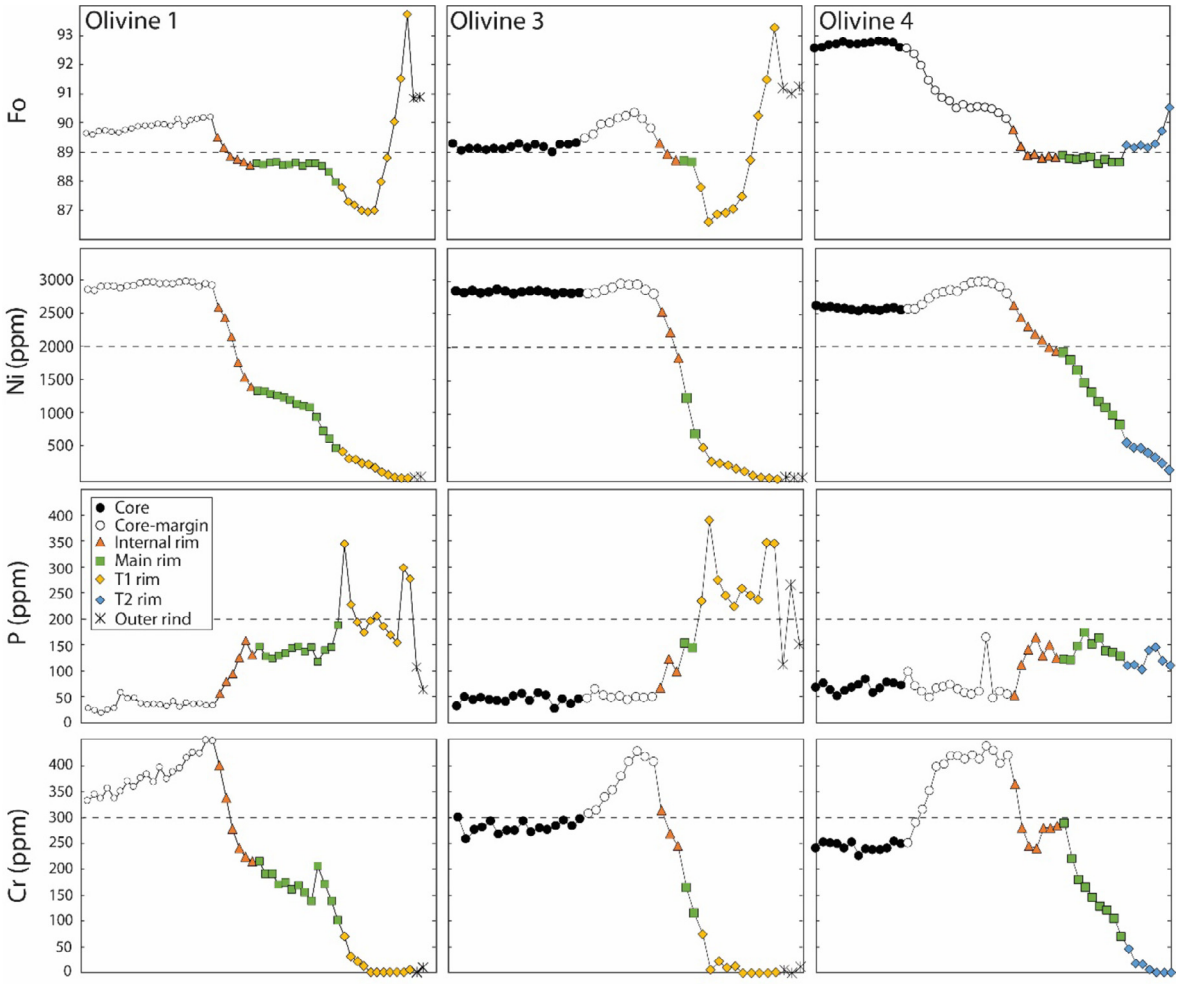

Fig. 3. Electron microprobe (EPMA) spot traverses for forsterite (Fo), Ni (ppm), P (ppm), and Cr (ppm) across olivine grains 1, 3 and 4 from the Benfontein kimberlite, South Africa. Olivine 1 traverse is the x-y traverse indicated in Fig. 1e. Olivine 3 traverse is x-y traverse indicated in Fig. 1a. Olivine 4 traverse is x-y traverse indicated in Fig. 2a.

The core-margin zones in both, type I and II, are gradational in BSE images (Figs. 1 and 2). Both type I and II olivine have core-margin zones with higher Ni, Ca, and Mn than the cores and display gradational changes that converge at a composition of $Fo_{90.5}$ with Ni-2900 ppm; Cr-430 ppm; Ti-130 ppm; Ca-530 ppm; Mn-880 ppm; and Al-90 ppm (Figs. 4 and 5). In contrast to these trace elements, P does not show any change and P-maps indicate that the core and core-margin have homogeneous low-P (<78 ppm) relative to the surrounding rims (Figs. 1 and 2).

3.2. Internal rim and main rim chemistry

The main rim in both olivine types is characterized by the occurrence of Cr-spinel inclusions. The contacts between the core-margins and the main rims are gradational (termed internal rim in Figs. 3–5) with a number of notable changes in olivine chemistry. In both the type I and II olivine the Fo content of the internal rims decreases from $Fo_{90.5}$ to $Fo_{88.7}$ along with decreasing Ni and Cr contents from 2900 ppm and 530 ppm to 1900 ppm and 260 ppm, respectively (Figs. 3 and 4). Calcium, Mn, P, and Ti all increase whereas Al decreases with decreasing Fo contents in the internal rim. This change marks the beginning of the main rim with a composition of: $Fo_{88.7}$, Ni-1900 ppm, Cr-260 ppm, Ti-176 ppm, Ca-560 ppm, Mn-1000 ppm, Al-50 ppm, and P-100 ppm (Figs. 2–5). The main rim displays a constant Fo content ($Fo_{88.7}$) with decreasing Ni and Cr, and increasing Ca, Ti, Mn, and P, and constant Al (Figs. 3–5).

3.3. Type I (T1) rim chemistry

The T1 rims are only present in type I olivine and are characterized by a sharp increase in P concentration. The P-rich olivine zones contain inclusions of ilmenite; no Cr-spinel inclusions are observed. The P contents range from 160 to 420 ppm and overall the T1 rim can be divided into three sub-zones based on P and Fo changes (labelled as 4a-4c in Fig. 6): (4a) inner P-rich (250–450 ppm) sub-zone with

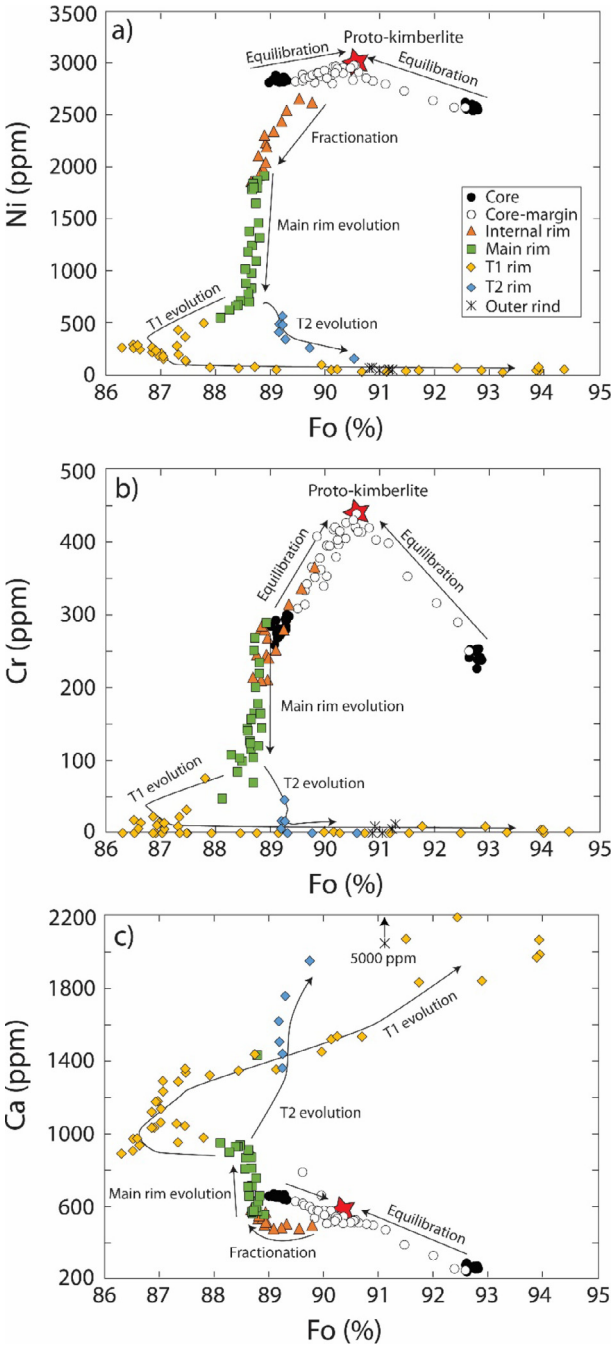

Fig. 4. All EPMA data for Benfontein olivine relative to Fo content. The red star represents the interpreted composition that is representative of the proto-/kimberlite melt responsible for early partial equilibration of olivine cores. (For interpretation of the references to colour in this figure legend, the reader is referred to the web version of this article.)

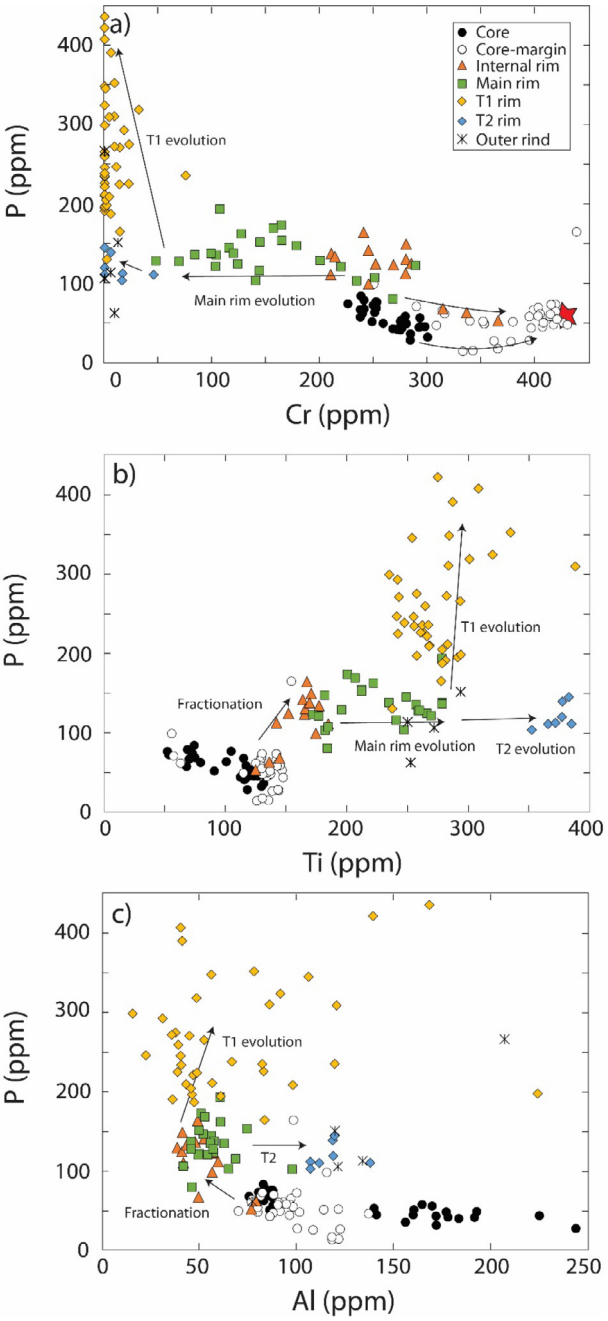

Fig. 5. All EPMA trace element data for Benfontein olivine relative to P concentrations. The red star represents the interpreted composition that is representative of the proto-/kimberlite melt responsible for early partial equilibration of olivine cores. (For interpretation of the references to colour in this figure legend, the reader is referred to the web version of this article.)

low Fo_{86-87}; (4b) a lower-P (<200 ppm) zone with Fo content of Fo_{87} and a gradational increase to Fo_{91} at the outer edge; (4c) an outer P-rich zone that shows increased P contents (~300 ppm) and a sharp increase in Fo from Fo_{91} up to Fo_{94}. Other minor/trace elements within this sub-zone such as Ca, Ti, Mn, show a constant increase whereas Ni and Cr show a constant decrease. The outer P-rich zone has abundant fine inclusions of P-rich material (Fig. 6). These P-rich inclusions are related to fine cracks that cross-cut the olivines where kimberlite has invaded and represent late-stage features rather than primary inclusions (Fig. 1f).

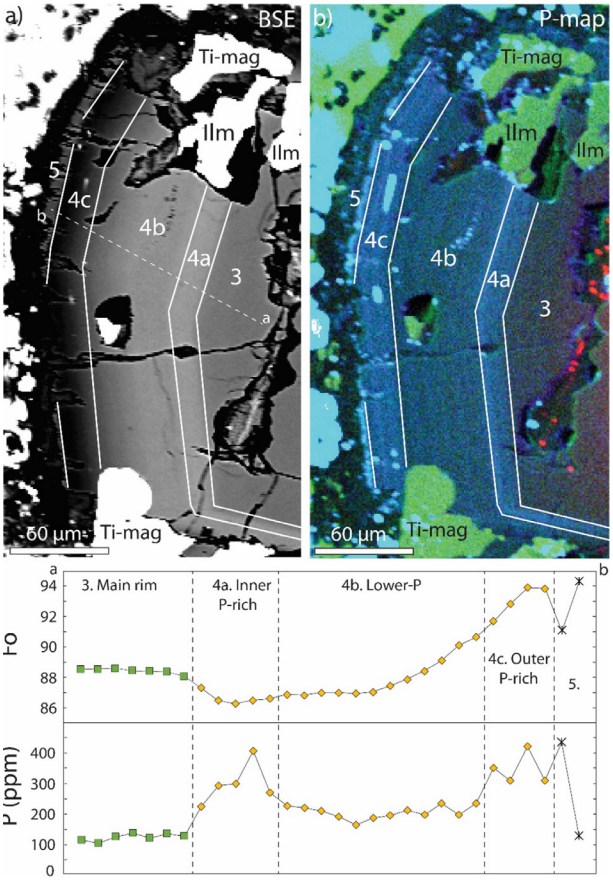

Fig. 6. BSE image and a-b EPMA traverse for a region of Benfontein olivine 3 illustrating the sub-division of the P-rich T1 rim (zones 4a–4c). The olivine zones are labelled 4–5 to be consistent with Fig. 1.

3.4. Type II (T2) rim chemistry

The T2 rims only occur in the type II olivine. They are observed surrounding the main rim. No gradational contact is noted in this case. The T2 rims have higher Fo ($Fo_{89.2}$) content than the main rims (Figs. 3–5). The Fo content increases up to $Fo_{90.5}$, and is accompanied by decreases Ni and Cr, increases in Ca, Mn, Ti, and Al, and constant P. The T2 rims contains the highest Ti contents ranging from 350 to 385 ppm and is clearly distinguished from rims of the type I olivine (Fig. 5b).

3.5. Rind (outer most zone) chemistry

The outer rind is observed in the type I olivine only in this study but does not occur continuously around the entire grains and is altered to serpentine. Thus, it is unclear whether this zone is only present in type I olivine or is just coincidentally preserved on the selected type I olivine. The outer rind shows a notable decrease in Fo from Fo_{94} to $Fo_{90.8}$ (Fig. 4). It is characterized by low concentrations of Ni (<250 ppm) and Cr (<20 ppm), variable P (50–150 ppm), and sharp increases in Ca (up to 5200 ppm) and Mn (up to 2500 ppm). Aluminum concentrations (~120 ppm) are higher than in the main rim and T1 rims (Fig. 5). In addition, it contains magnetite-rich spinel.

4. DISCUSSION

4.1. Internal diffusion controlled zoning and implications for proto-kimberlite melt association and early liquidus olivine crystallization

Phosphorous mapping in the Benfontein olivine grains shows a homogeneously depleted core zone with P concentrations of <78 ppm, which is similar to the range of P concentrations of <71 ppm for olivine from kimberlite-derived mantle xenoliths in South Africa, reported by De Hoog et al. (2010). The core-margin zones form part of this P-poor core (Figs. 1 and 2) and no increase is observed for P with increasing concentrations of other trace elements such as Cr, Ni, and Ti in these zones. This is consistent with the extremely slow (i.e., essentially immobile) nature of P diffusion in olivine (e.g., Milman-Barris et al., 2008; Welsch et al., 2014; Shea et al., 2015; Lynn et al., 2018) and the P-poor nature of mantle olivine (e.g., Mallmann et al., 2009; De Hoog et al., 2010). In addition, the P-poor cores commonly have rounded shapes relative to the euhedral rim zones and suggests resorption of the olivine core (Figs. 1e and 2a). Thus, the P-poor core represents the outline of the original mantle xenocryst grain whereas the gradational change to the core-margin zone noted by increases of other trace elements (e.g., Cr) represents a diffusion zone, implying partial equilibration of the xenocrystic cores with a melt phase preceding olivine crystallization in the proto-/kimberlite melt.

The definition of a clear zone related to diffusion and partial equilibration (i.e., core-margin zone) allows us to define the olivine chemistry representative of the early stage of melt evolution related to kimberlite petrogenesis. Fe-Mg diffusion in olivine is a rapid process (equilibration in days to years for 5–300 µm grain; see Lynn et al., 2018 for summary of diffusion rates) and preservation of the core-margin equilibration zones in Fo content implies formation immediately preceding the kimberlite ascent to the surface. The olivine chemistry in this study, representative of the early melt responsible for core-margin partial equilibration, is estimated using the convergence of the core-margin zonation trends indicated by the red star in Figs. 4 and 5. The olivine at this convergence point has $Fo_{90.5}$, Ni-2900 ppm; Cr-430 ppm; Ti-130 ppm; Ca-530 ppm; Mn-880 ppm; and Al-90 ppm. This olivine chemistry is similar to Cr-rich olivine megacrysts reported in southern African kimberlites, which typically have high-Cr (410–750 ppm) contents and high-Fo ($Fo_{90.6}$-$Fo_{91.9}$) contents (Eggler et al., 1979) relative to the Cr-poor megacryst suite represented by the Monastery kimberlite olivine megacrysts with low-Cr (<100 ppm) and low-Fo ($Fo_{<88}$) contents (e.g., Gurney et al., 1979; Bell et al., 2004; Howarth, 2018).

Changes in the geochemistry noted from Cr-poor to Cr-rich megacrysts (including increases in Cr contents) has been interpreted to result from the assimilation of lithospheric mantle material by a proto-kimberlite melt toward the base of the lithospheric mantle (e.g., Bussweiler et al.,

2015; Janney and Bell, 2017). The dissolution/assimilation of orthopyroxene in the lithospheric mantle has been suggested to be a major process in the generation of kimberlite magmas (e.g., Brett et al., 2009; Russell et al., 2012; Kamenetsky and Yaxley, 2015) and is reflected by increased Cr contents in olivine due to high-Cr contents in orthopyroxene (e.g., Bussweiler et al., 2015). The Cr-rich, $Fo_{90.5}$ olivine core-margin zones in this study are consistent with these previous studies and are interpreted to represents partial equilibration with a Cr-rich proto- /kimberlite melt within the lithospheric mantle after a previous stage of orthopyroxene assimilation. This interpretation further suggests an intimate association between kimberlite and proto-kimberlite melts in the lithospheric mantle (e.g., Nowell et al., 2004; Howarth and Buttner, 2019) and confirms a close petrogenetic link between megacrystic and kimberlitic olivine where both Fe-rich and Mg-rich olivine xenocrystic cores in kimberlitic olivine may be sourced in part from olivine megacrysts belonging to the Cr-rich (Mg-rich $> Fo_{90}$) and Cr-poor (Fe-rich $< Fo_{88}$) groups (e.g., Moore and Costin, 2016).

Internal zonation of kimberlitic olivine was first observed by Fedortchouk and Canil (2004) and Kamenetsky et al. (2008) and subsequently has been identified in a number of more recent studies (e.g., Bussweiler et al., 2015; Cordier et al., 2015; Sobolev et al., 2015; Lim et al., 2018; Soltys et al., 2018). In these cases, the internal zones were defined by compositions intermediate between the core and the main rim zones and were attributed to either diffusional equilibration with melt (Pilbeam et al., 2013), fluid-assisted deformation and recrystallization (Cordier et al., 2015), or early liquidus olivine crystallization after or coeval with orthopyroxene crystallization (Giuliani and Foley, 2016). It must be emphasized here that the core-margin zones observed in this study do not represent intermediate compositions between the cores and main rim zone but rather between the xenocrystic core and the inferred proto-kimberlite melt composition and are not like those described in the aforementioned studies. Rather, the internal rim zone described in this study (Figs. 3–5) observed between the main rim trend and the core-margin zone defines a zone of intermediate composition between the cores and the main rim olivine zone and thus are equivalent to the internal zonations described in previous studies discussed above. This internal zone at Benfontein is characterized by an increase in P concentration, which we interpret to reflect the first stage of liquidus olivine crystallization in the system and we favour the interpretations of Giuliani and Foley (2016) with regard to internal zones with composition intermediate between core and the main rim olivine zones.

4.2. Concentric oscillatory olivine growth

Olivine in this study shows abrupt increases and decreases in Fo contents between the different rim zones, which correlate with changes in P concentrations (Figs. 1 and 2). Increases in Fo contents in olivine (i.e., reverse zoning) is commonly attributed to magma mixing/recharge where a new, more primitive magma enters an existing magma chamber leading to olivine rims with increased Fo and Ni contents (e.g., Streck, 2008). However, Ni in Benfontein olivine from this study decreases constantly across the multiple olivine rim zones and is very low (<500 ppm) in the P-rich zone (T1 rim). This is consistent with the compatible behavior of Ni during olivine fractionation and inconsistent with magma mixing/recharge. The Fo and Ni variations generally correspond with the exception of a sharp increase in Fo contents at the outer portion of the T1 rim zone (Fig. 3). Such increases in Fo contents in the outer rims/rinds of kimberlitic olivine in the past have been interpreted to reflect late stage increase in fO_2 conditions (e.g., Bussweiler et al., 2015; Howarth and Taylor, 2016; Giuliani, 2018). Similar Mg-rich olivine have been reported in basaltic magmas, which have been attributed to unusually high oxidation state (e.g., Cortes et al., 2006; Blondes et al., 2012). Such an increase in Fo content in olivine is due to the incompatible nature of Fe^{3+} in olivine (Roeder and Emslie, 1970). With the resultant increase of Fe^{3+}/Fe^{2+} ratio in the melt at high oxidation state, less Fe^{2+} enters the olivine and thus, Fo-rich olivine forms. The increase in olivine Fo for the Benfontein olivine rinds coincides with the presence of magnetite-rich spinel inclusions in the outer portions of the olivine, again indicating an increase in fO_2 conditions at this state of magma evolution. Therefore, late-stage decoupling of Fo-Ni is likely an effect of a late-stage increase in oxidation state of the melt. Ultimately, magma mixing/recharge is unlikely the source for multiple Fo and P zones observed for the Benfontein olivine. This interpretation is also consistent with the interpretation of many recent studies where such concentric P zoning is observed (e.g., Milman-Barris et al., 2008; Shearer et al., 2013; Baziotis et al., 2017) who suggested that magma mixing/recharge is unlikely a controlling process in P zoning in olivine.

Phosphorous, unlike other incompatible elements in olivine, diffuses extremely slowly and is an order of magnitude slower than other slow diffusing elements such as Cr (e.g., Welsch et al., 2014; Shea et al., 2015; Watson et al., 2015). Phosphorous is also an incompatible element ($D^{olivine\text{-}melt} = 0.1–0.01$) in olivine and is incorporated in low concentrations (<0.01 wt.%) during slow growth rate ($<10^{-9}$ m/sec) at near-equilibrium conditions (e.g., Milman-Barris et al, 2008; Grant and Kohn, 2013; Baziotis et al., 2017). The concentration of P in olivine during equilibrium growth is dependent on the P concentration of the melt (Milman-Barris et al., 2008; Boesenberg and Hewins, 2010), as is true for most minor/trace elements in olivine such as Ni, Ca, and Ti. P-enriched olivine has been attributed to two possible processes. (1) Fast crystallization under equilibrium conditions resulting in P enriched boundary layers surrounding olivine and ultimately enrichment of P in olivine. Such a process was observed in the experiments of Milman-Barris et al. (2008), however, the enrichment of P in the boundary layer is only ~20 % relative to the far field melt. This cannot account for the enriched P zones for the Benfontein olivine from ~125 ppm up to 400–450 ppm, consistent with the interpretations of Milman-Barris et al. (2008) who also suggested that such a process may contribute but is not the control-

ling factor in P-enriched olivine zones. (2) Rapid growth under disequilibrium conditions also known as 'solute trapping' allows for the uptake of larger concentrations of incompatible elements in olivine, such as P (e.g., Milman-Barris et al., 2008; Welsch et al., 2014; Shea et al., 2015). Solute trapping is essentially a process whereby olivine growth rate is greater than the rate at which a cation can diffuse away from the crystal-melt interface (e.g., Reitano et al., 1994; Charach and Keizman, 1996). Such a process is believed to be particularly important for slow diffusing elements such as P that can be trapped by rapid growth of olivine. This is a disequilibrium process and can result in an increase of the olivine-melt partition coefficient to values up to 0.4–0.5 (e.g., Goodrich, 1984; Milman-Barris et al., 2008). Baziotis et al. (2017) modelled such conditions at varying olivine-melt partition co-efficients (0.1–0.01) for P and showed that growth rates on the order of 10^{-8} m/sec or greater are required to account for enrichment of P in olivine. Such growth rates are an order of magnitude greater than those modelled for equilibrium growth (e.g., Baziotis et al., 2017).

No relationship is observed between P and other incompatible elements such as Cr and Al for the Benfontein olivine, however, the sharp increases in P do correspond with changes in Fo contents in the multiple rim zones surrounding the olivine cores (Figs. 1 and 2). Two distinct P-rich zones are observed in olivine grains 1 and 3 (Figs. 2 and 6). The inner P-rich zone (4a in Fig. 6) is correlated with a decrease in Fo content from Fo_{89} in the main rim to $Fo_{86\text{-}87}$ in the P-rich T1 rim zone. In contrast, the outer P-rich T1 rim zone (4c in Fig. 6) corresponds to an increase in Fo contents up to Fo_{93}. The gradational increase in Fo content between the lower P zone (Zone 4b; Fig. 6) and outer P-rich zone (Zone 4c; Fig. 6) suggests some Fe-Mg equilibration between these zones, however, ultimately the P change correlates with changes in Fo with only minor evidence for diffusion between the different zones. The overall P zoning observed for the Benfontein type I olivine is similar to the concentric oscillatory P-rich zones and multiple closely spaced P-rich bands described by Milman-Barris et al. (2008) and illustrated in their Figs. 1b and 2b. Such P-zoning patterns were not produced in the experiments of Milman-Barris et al. (2008) and they interpreted these features to represent changes in growth rate related to extrinsic factors (temperature, pressure, pH_2O, fO_2 etc.) during magma evolution. In the case of the Benfontein olivine, the P-enriched zones form after an early stage of equilibrium olivine crystallization represented by the low-P (100–150 ppm) main rim zone (Zone 3; Fig. 6). Thus, the enriched P-zones are not a function of the onset of liquidus olivine crystallization through undercooling such as in other examples where dendritic internal crystal architecture is preserved by P-rich zones (e.g., Welsch et al., 2014; Baziotis et al., 2017; Xing et al., 2017). Instead, the enriched P-zones here represent a later stage of growth rate increase during magma evolution, which results in an increase in P concentration through the mechanism of solute trapping. Therefore, we suggest that the concentric P-poor to P-rich zones of the Benfontein olivine are tracking changes in growth rate during the evolution of the kimberlite magma *en route* to the surface.

The oscillatory nature of the P-zoning in the type I Benfontein olivine is interpreted to represent staged kimberlite ascent, likely in the upper-crust, by multiple rapid stages of ascent resulting in rapid decreases in pressure-temperature and resultant increased growth rate and disequilibrium olivine growth characterized by increased olivine-melt partition coefficients for phosphorous through solute trapping. Between each rapid ascent 'burp' a stage of magma ponding likely occurred resulting in equilibrium low-P olivine growth. A possible controlling mechanism for such staged ascent was presented as an early model for kimberlite magma emplacement in southern Africa by Clement (1982) (i.e., embryonic pipe model) and subsequently adopted by numerous other studies (e.g., Field and Scott Smith, 1999; Howarth and Skinner, 2013). In this model of embryonic pipe development, kimberlite magma stalls at more competent crustal units (such as dolerite sills for Kaapvaal craton kimberlites), followed by slow hydraulic fracturing until the kimberlite breaches the sill and subsequent continuation of rapid ascent. Such changes in ascent rate may also result in changes from equilibrium to disequilibrium olivine growth due to episodic rapid pressure-temperature decrease once lithological barriers are overcome, as observed in changes in the P contents of the olivine described in this study. Such a process is illustrated in our summary model for olivine growth in Fig. 7.

4.3. Late-stage magma mixing

The core-margin (zone 2 in Figs. 1 and 2) and main rim (zone 3 in Figs. 1 and 2) zones for both the type I and type II olivine have identical chemistries, suggesting similar early stages of petrogenesis. However, the T1 and T2 rim zones (zone 4 in Figs. 1 and 2) display different chemical trends that indicate different late-stage petrogenesis. The T1 rim zone is characterized by oscillatory Fo and P zones and are interpreted to form through staged upward intrusion. The T2 rim zone is characterized by high-Ti content relative to T1 and constant low-P. Thus, the T2 rim zone does not undergo rapid disequilibrium growth stages as observed for T1 olivine. The increase of Ti in the T2 rim zone relative to the T1 is consistent with the absence of ilmenite in T2 olivine whereas ilmenite chadacrysts in T1 olivine are observed within the T1 rim zone (Fig. 6). Thus, the constant Ti in T1 rim zones and increase in Ti in the T2 rim zones is interpreted to reflect ilmenite crystallization or lack thereof and ultimately a different melt petrogenesis in each case. The amount of ilmenite in typical kimberlites varies widely from up to 10 wt.% to kimberlites devoid of ilmenite and different kimberlites within a single body commonly containing varying ilmenite proportions (Mitchell, 1986). Thus, the presence/absence of ilmenite in the T1 and T2 Benfontein olivine is a common feature in kimberlite intrusions and is not unusual.

The presence of both type I and II olivine within the same macrocrystic kimberlite sample indicates late-stage magma mixing after the formation of the T1 and T2 rim zones. The two separate pulses of magma underwent identical early stages of melt petrogenesis characterized by proto-kimberlite melt metasomatism (core-margin zone)

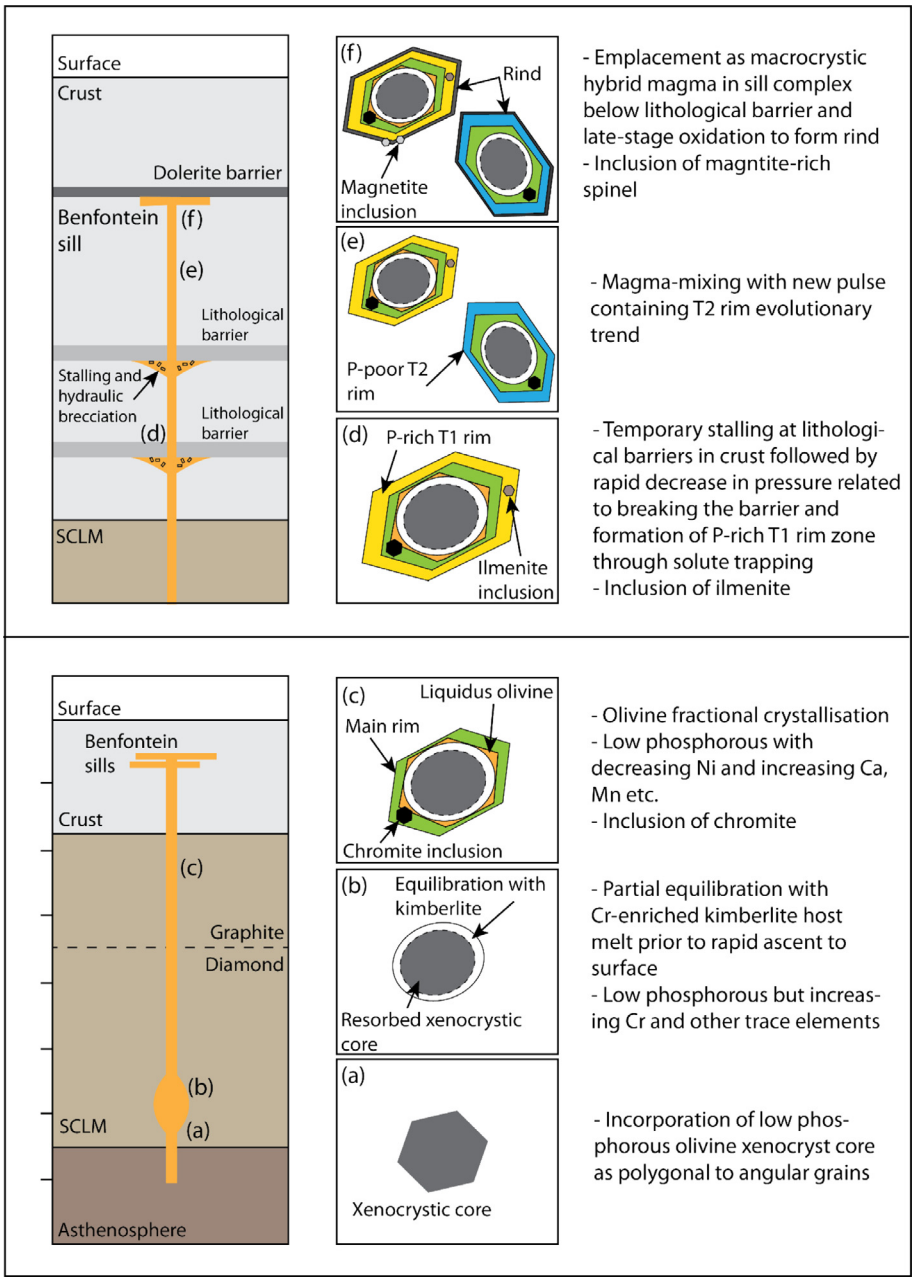

Fig. 7. Simplified illustration of the envisioned stages of kimberlite petrogenesis based on the chemical zoning of olivine, as discussed in detail in the text Section 4.4.

and subsequent evolution through olivine (decreasing Ni) and chromite (decreasing Cr) fractionation (main rim zone 3 in Figs. 1 and 2). The T1 rim zone evolution was controlled by alternating equilibrium and disequilibrium growth whereas the T2 rim zone was characterized by the absence of concurrent ilmenite crystallization. Late-stage magma mixing is consistent with the formation of the Benfontein kimberlite sills through multiple pulses of magma (e.g., Dawson and Hawthorne, 1973; Abersteiner et al., 2019). Thus, P-zoning in kimberlitic olivine highlights the necessity for careful, high-spatial resolution mapping and high-precision quantitative spot analyses as a further, independent tool that can be used in discriminating multiple populations of olivine within individual samples. Identification of multiple olivine populations further highlights the hybrid nature of kimberlite magmas and the difficulty in constraining the parent melt composition.

4.4. Model for olivine formation during kimberlite petrogenesis (Benfontein)

Here we present a summary of the formation and evolution of the Benfontein olivine. Six stages of olivine formation are discussed and illustrated (a)–(f) in Fig. 7.

(a) Proto-kimberlite melt ascends into the base of the lithospheric mantle where it incorporates olivine as xenocryst grains and at the same time assimilates orthopyroxene, which is highly unstable in kimberlite melt (e.g., Russell et al., 2012; Kamenetsky and Yaxley, 2015). Prior to significant orthopyroxene assimilation the proto-kimberlite would crystallize relatively Fe-rich olivines such as those representative of the Cr-poor megacryst suite (i.e., Monastery olivine $<Fo_{88}$; Gurney et al., 1979; Bell et al., 2004; Howarth, 2018). The early proto-kimberlite melt is enriched in Cr during progressive orthopyroxene assimilation and evolves toward more Mg-rich compositions, which are represented by the Cr-rich megacryst suite with more Mg-rich compositions ($>Fo_{90}$). We discriminate here between proto-kimberlite as prior to orthopyroxene enrichment and kimberlite proper after orthopyroxene assimilation.

(b) Olivine xenocryst grains are partially resorbed resulting in rounded morphology and partially equilibrate with Cr-enriched kimberlite melt. The olivine equilibration zones trend toward chemistry similar to that of typical Cr-rich olivine megacrysts, in the case of Benfontein, with Fo content of 90.5 and Cr content of ~430 ppm. Phosphorous is notable low and similar to that of the xenocryst core, due to the very slow diffusivity of P relative to other elements.

(c) The first stage of liquidus olivine crystallization is represented by an increase in P and the occurrence of chromite chadacrysts. This zone is characterized by a decrease in Fo, Ni, and Cr due to olivine and chromite fractionation. The early liquidus olivine transitions into the main rim zone characterized by Fo contents buffered at $Fo_{88.8}$. Several models have been suggested in the current literature to account for the buffered Fo contents of olivine rims. These include: (1) high Fe-Mg distribution coefficient typical of carbonate-rich melt (e.g., Kamenetsky et al., 2008; Moore, 2017); (2) fractionation of olivine and minor ilmenite coupled with orthopyroxene assimilation (Pilbeam et al., 2013); and (3) low Fe-Mg distribution coefficient but high olivine-melt partition coefficient (Cordier et al., 2015). For detailed discussion on these processes the reader is referred to the review paper of Giuliani (2018).

(d) The kimberlite melt enters the crust and temporarily stalls at more competent lithological layers (e.g., Clement, 1982; Field and Scott Smith, 1999; Skinner, 2008; Howarth and Skinner, 2013). The lithological barrier is overcome through hydraulic fracturing due to volatile exsolution and resultant increase in pressure of the system. Once the lithological barrier is overcome the kimberlite melt then ascends rapidly through the crust. The rapid change in pressure after breakthrough is envisioned to result in increased growth rate of olivine and incorporation of P in excess of equilibrium growth through the process of solute trapping. This process may be repeated multiple times depending on the crustal sequence and lithological barriers. In addition, chromite is no longer the oxide phase crystallizing and is replaced by the crystallization and incorporation of ilmenite chadacrysts into the growing olivine.

(e) At some point in the crust, the original kimberlite magma mixed with a new pulse. The latter pulse is characterized by olivine with different late-stage evolution and without the formation of P-enriched zones.

(f) The last stage of olivine evolution is accompanied by an increase in oxidation conditions resulting in the formation of Fo-rich rinds. In addition, the dominant oxide is magnetite-rich spinel at this stage, consistent with higher oxidation conditions.

4.5. Implications for the growth of igneous olivine

Recent work has shown that olivine commonly grows as dendritic P-rich crystals under disequilibrium conditions that are subsequently filled-in during a later equilibrium crystallization stage to form euhedral crystals (e.g., Milman-Barris et al., 2008; Welsch et al., 2014; Shea et al., 2015; Baziotis et al., 2017; Xing et al., 2017). Welsch et al. (2014) showed that P-rich dendritic branches located near the margins of olivine are in fact older than P-poor inner zones. Thus, an important implication of work presented here on the Benfontein olivine is that olivine can also grow in concentric growth zones and that dendritic growth is not a ubiquitous feature of P-rich olivine.

A major question arising from recent work (e.g., Welsch et al., 2014; Shea et al., 2015) is whether there are instances where major element zoning in olivine can be demonstrated to be unequivocally produced by crystal growth. The best possible way to demonstrate major element growth zoning is by using a multi-element approach and correlation between fast (Fe-Mg), slow (Ni, Cr) and very slow (P) diffusing elements. The correlated changes in Fo and P in the Benfontein type I olivine indicate that Fo zoning in olivine can indeed be produced by stages of crystal growth and are not a feature of diffusive re-equilibration. Thus, the Benfontein olivine in this study represent a rare example of major element zoning in olivine formed through stages of crystal growth induced by rapid changes in temperature-pressure-fO_2 during magma evolution.

Experimental studies along with studies of natural samples have shown a positive correlation between slow diffusing elements such as P-Al-Cr (e.g., Milman-Barris et al., 2008; McCanta et al., 2016), however, natural olivine grains do not always show such correlations (e.g., Milman-Barris et al., 2008; Shearer et al., 2013; Baziotis et al., 2017; Ersoy et al., 2019), consistent with observations in this study. The preservation of the Fo zoning (Fe-Mg fast diffusing) in the Benfontein olivine and correlation with P (slow diffusing) suggests that preservation of Al and Cr is also likely and that the absence of any correlation between P and Al-Cr is a primary feature of the olivine and not a result of later diffusion and equilibration of the olivine. Such an interpretation leads to the question of why oscillatory zoning is observed in Fo and P but no other elements that diffusive on timescales intermediate between Fo and P. One possible

answer to this question is rapid changes in both growth rate (tracked by P) as well as fO_2. Because Fe^{3+} is incompatible in olivine (e.g., Roeder and Emslie, 1970), at higher fO_2 conditions less Fe is taken into the crystal structure and thus more Fo-rich olivine crystallizes. Changes in Fo content of the type I olivine is correlated with changes in the oxide inclusions from chromite (main rim) to ilmenite (P-rich rim) and finally Ti-magnetite (outer rim) (Fig. 1). Such an increase in fO_2 during kimberlite evolution is also shown by decreases in V/Sc concentrations from core to margin (e.g., Howarth and Taylor, 2016; Giuliani, 2018) and consistent with the oxide chadacryst observations in this study. Thus, we suggest that the rapid changes in Fo contents of the olivine is tracking changes in fO_2 conditions during the evolution of the kimberlite and coincides with the growth rate changes observed in P zoning.

5. CONCLUSIONS

We report multiple P-poor and P-rich zones in kimberlitic olivine. P-poor core zones represent the outline of the original mantle xenocryst whereas low-P gradational core-margin zones characterized by the increase of Cr, Ni and other minor/trace elements represent equilibration zones. Thus, phosphorous zoning in kimberlitic olivine has great potential in discriminating between early stages of core equilibration prior to olivine crystal growth. The low-P xenocrystic cores are subsequently surrounded by multiple crystal growth zones characterized by correlated changes in Fo and P. The P-enriched zones are interpreted to reflect stages of rapid disequilibrium growth and resultant high P concentrations through solute trapping controlled by extrinsic process such as changes in pressure-temperatures during the evolution of the kimberlite magma. The P-poor zones are interpreted to represent stages of equilibrium growth.

The correlated changes between fast Fe-Mg (i.e., Fo content) and slow P diffusing elements suggest that crystal growth can result in major element zoning in olivine. In addition, multiple concentric zones in olivine can form by successive stages of olivine crystal growth.

Furthermore, we suggest the following elements in olivine to be useful in understanding various aspects of kimberlite crystallization:

1. Phosphorous can be used to discriminate diffusion versus crystal growth for core-margin gradational (also called transitional zones) and tracks stages of equilibrium versus disequilibrium growth in surrounding crystal growth zones.
2. Multi-element olivine zonation trends of the core-margin equilibration zones converge at a point source in X-Y scatter plots and can effectively be used to constrain the earliest stage of kimberlite melt development in the mantle. The notable increase in Cr contents and similarity with Cr-rich megacrysts may suggest a common origin.
3. Nickel and Cr effectively track the fractional crystallization of olivine and Cr-spinel during kimberlite evolution.
4. Titanium effectively tracks the onset of ilmenite crystallization. In the case of the type II Benfontein olivine, ilmenite inclusions are not observed and the outer T2 melt evolution zone is characterized by continued increase in Ti during late-stage crystallization. In contrast, the type I olivine contain ilmenite inclusions within the inner P-rich zone and increase in Ti is terminated at this stage of olivine growth.

ACKNOWLEDGEMENTS

The Benfontein kimberlite sample analyzed in this study was kindly loaned from the John Gurney mantle xenolith collection at the University of Cape Town, South Africa. We would like to thank Vadim Kamenetsky and two anonymous reviewers for detailed and very helpful comments, which greatly improved the quality of the manuscript. We would also like to thank James Day for very efficient and helpful editorial handling of the manuscript. J.G. likes to acknowledge funding from her Rutgers start-up grant.

APPENDIX A. SUPPLEMENTARY MATERIAL

Supplementary data to this article can be found online at https://doi.org/10.1016/j.gca.2019.08.006.

REFERENCES

Abersteiner A., Kamenetsky V. S., Goemann K., Giuliani A., Howarth G. H., Castillo-Oliver M. and Cherry A. (2019) Composition and emplacement of the Benfontein kimberlite sill complex (Kimberley, South Africa): textural, petrographic and melt inclusion constraints. *Lithos* **324**, 297–314.

Arndt N. T., Guitreau M., Boullier A. M., Le Roex A., Tommasi A., Cordier P. and Sobolev A. (2010) Olivine, and the origin of kimberlite. *J. Petrol.* **51**(3), 573–602.

Baziotis I., Asimow P. D., Ntaflos T., Boyce J. W., McCubbin F. M., Koroneos A. and Klemme S. (2017) Phosphorus zoning as a recorder of crystal growth kinetics: application to second-generation olivine in mantle xenoliths from the Cima Volcanic Field. *Contrib. Miner. Petrol.* **172**(7), 58.

Bell D. R., Rossman G. R. and Moore R. O. (2004) Abundance and partitioning of OH in a high-pressure magmatic system: megacrysts from the Monastery kimberlite, South Africa. *J. Petrol.* **45**(8), 1539–1564.

Blondes M. S., Brandon M. T., Reiners P. W., Page F. Z. and Kita N. T. (2012) Generation of forsteritic olivine (Fo99· 8) by subsolidus oxidation in basaltic Flows. *J. Petrol.* **53**(5), 971–984.

Boesenberg J. S. and Hewins R. H. (2010) An experimental investigation into the metastable formation of phosphoran olivine and pyroxene. *Geochim. Cosmochim. Acta* **74**(6), 1923–1941.

Brett R. C., Russell J. K. and Moss S. (2009) Origin of olivine in kimberlite: phenocryst or impostor?. *Lithos* **112** 201–212.

Bussweiler Y., Foley S. F., Prelević D. and Jacob D. E. (2015) The olivine macrocryst problem: new insights from minor and trace element compositions of olivine from Lac de Gras kimberlites, Canada. *Lithos* **220**, 238–252.

Clement C. R., Skinner E. M. W. and Smith B. S. (1984) Kimberlite redefined. *J. Geol.* **92**(2), 223–228.

Clement, C. R. (1982). A comparative geological study of some major kimberlite pipes in the Northern Cape and Orange Free State (Doctoral dissertation). University of Cape Town.

Charach C. and Keizman Y. (1996) Solute trapping effects in planar isothermal solidification of dilute binary alloys. *Phys. Rev. E* **54**(1), 588.

Cordier C., Sauzeat L., Arndt N. T., Boullier A. M., Batanova V. and Barou F. (2015) Metasomatism of the lithospheric mantle immediately precedes kimberlite eruption: new evidence from olivine composition and microstructures. *J. Petrol.* **56**(9), 1775–1796.

Cortés J. A., Wilson M., Condliffe E. and Francalanci L. (2006) The occurrence of forsterite and highly oxidizing conditions in basaltic lavas from Stromboli volcano, Italy. *J. Petrol.* **47**(7), 1345–1373.

Costa F., Dohmen R. and Chakraborty S. (2008) Time scales of magmatic processes from modeling the zoning patterns of crystals. *Rev. Mineral. Geochem.* **69**(1), 545–594.

Costa F. and Chakraborty S. (2004) Decadal time gaps between mafic intrusion and silicic eruption obtained from chemical zoning patterns in olivine. *Earth Planet. Sci. Lett.* **227**(3–4), 517–530.

Dawson J. B. and Hawthorne J. B. (1973) Magmatic sedimentation and carbonatitic differentiation in kimberlite sills at Benfontein, South Africa. *J. Geol. Soc.* **129**(1), 61–85.

De Hoog J. C., Gall L. and Cornell D. H. (2010) Trace-element geochemistry of mantle olivine and application to mantle petrogenesis and geothermobarometry. *Chem. Geol.* **270**(1), 196–215.

Donovan J. J. (2012) *Probe for EPMA: Acquisition, Automation and Analysis edited*, Enterprise Edition. Probe Software Inc, Eugene.

Eggler D. H., McCallum M. E. H. and Smith C. B. (1979) Megacryst assemblages in Kimberlite from Northern Colorado and Southern Wyoming: petrology, geothermometry-barometry, and areal distribution. *The Mantle Sample: Inclusion in Kimberlites and Other Volcanics* **16**, 213–226.

Elardo S. M. and Shearer, Jr., C. K. (2014) Magma chamber dynamics recorded by oscillatory zoning in pyroxene and olivine phenocrysts in basaltic lunar meteorite Northwest Africa 032. *Am. Mineral.* **99**(2–3), 355–368.

Ersoy Ö., Nikogosian I. K., van Bergen M. J. and Mason P. R. D. (2019) Phosphorous incorporation in olivine crystallized from potassium-rich magmas. *Geochim. Cosmochim. Acta* **253**, 63–83.

Fedortchouk Y. and Canil D. (2004) Intensive variables in kimberlite magmas, Lac de Gras, Canada and implications for diamond survival. *J. Petrol.* **45**(9), 1725–1745.

Field, M. and Scott Smith, B. H. (1999). Contrasting geology and near-surface emplacement of kimberlite pipes in southern Africa and Canada. In Proceedings of the 7th international kimberlite conference. Red Roof Design Cape Town, vol. 1, pp. 214–237.

Foley S. F., Prelevic D., Rehfeldt T. and Jacob D. E. (2013) Minor and trace elements in olivines as probes into early igneous and mantle melting processes. *Earth Planet. Sci. Lett.* **363**, 181–191.

Giuliani A. (2018) Insights into kimberlite petrogenesis and mantle metasomatism from a review of the compositional zoning of olivine in kimberlites worldwide. *Lithos* **312**, 322–342.

Giuliani A., Soltys A., Phillips D., Kamenetsky V. S., Maas R., Goemann K. and Griffin W. L. (2017) The final stages of kimberlite petrogenesis: petrography, mineral chemistry, melt inclusions and Sr-CO isotope geochemistry of the Bultfontein kimberlite (Kimberley, South Africa). *Chem. Geol.* **455**, 342–356.

Giuliani A. and Foley S. F. (2016) The geochemical complexity of kimberlite rocks and their olivine populations: a comment on Cordier et al. (Journal of Petrology, 56, 1775–1796, 2015). *J. Petrol.* **57**(5), 921–926.

Goodrich C. A. (1984) Phosphoran pyroxene and olivine in silicate inclusions in natural iron-carbon alloy, Disko Island, Greenland. *Geochim. Cosmochim. Acta* **48**(5), 1115–1126.

Gordeychik B., Churikova T., Kronz A., Sundermeyer C., Simakin A. and Wörner G. (2018) Growth of, and diffusion in, olivine in ultra-fast ascending basalt magmas from Shiveluch volcano. *Sci. Rep.* **8**(1), 11775.

Grant T. B. and Kohn S. C. (2013) Phosphorus partitioning between olivine and melt: an experimental study in the system Mg2SiO4-Ca2Al2Si2O9-NaAlSi3O8-Mg3 (PO4) 2. *Am. Mineral.* **98**(10), 1860–1869.

Gross J., Filiberto J., Herd C. D., Daswani M. M., Schwenzer S. P. and Treiman A. H. (2013) Petrography, mineral chemistry, and crystallization history of olivine-phyric shergottite NWA 6234: a new melt composition. *Meteorit. Planet. Sci.* **48**(5), 854–871.

Gurney J. J., Jakob W. R. O. and Dawson J. B. (1979) Megacrysts from the Monastery kimberlite pipe, South Africa. *The Mantle Sample: Inclusion in Kimberlites and Other Volcanics* **16**, 227–243.

Herzberg C., Vidito C. and Starkey N. A. (2016) Nickel–cobalt contents of olivine record origins of mantle peridotite and related rocks. *Am. Mineral.* **101**(9), 1952–1966.

Howarth G. H. and Büttner S. H. (2019) New constraints on archetypal South African kimberlite petrogenesis from quenched glass-rich melt inclusions in olivine megacrysts. *Gondwana Res.* **68**, 116–126.

Howarth G. H. (2018) Olivine megacryst chemistry, Monastery kimberlite: constraints on the mineralogy of the HIMU mantle reservoir in southern Africa. *Lithos* **314**, 658–668.

Howarth G. H. and Harris C. (2017) Discriminating between pyroxenite and peridotite sources for continental flood basalts (CFB) in southern Africa using olivine chemistry. *Earth Planet. Sci. Lett.* **475**, 143–151.

Howarth G. H. and Taylor L. A. (2016) Multi-stage kimberlite evolution tracked in zoned olivine from the Benfontein sill, South Africa. *Lithos* **262**, 384–397.

Howarth G. H. and Skinner E. M. W. (2013) Sub-volcanic development of kimberlite pipes: evidence from the Lace and Voorspoed (Group II) kimberlites, South Africa. *J. Volcanol. Geoth. Res.* **268**, 1–16.

Howarth G. H., Michael E., Skinner W. and Prevec S. A. (2011) Petrology of the hypabyssal kimberlite of the Kroonstad group II kimberlite (orangeite) cluster, South Africa: Evolution of the magma within the cluster. *Lithos* **125**(1–2), 795–808.

Janney, P.E., Bell, D.R., 2017. Hidden reservoirs in the continental lithosphere? Evidence from Hf-Sr-Nd-Pb isotopes in Southern African Kimberlite Megacrysts. In 11th International kimberlite conference extended abstract no. 11IKC-4630, p. 2017.

Kamenetsky V. S. and Yaxley G. M. (2015) Carbonate–silicate liquid immiscibility in the mantle propels kimberlite magma ascent. *Geochim. Cosmochim. Acta* **158**, 48–56.

Kamenetsky V. S., Kamenetsky M. B., Sobolev A. V., Golovin A. V., Demouchy S., Faure K., Sharygin V. V. and Kuzmin D. V. (2007) Olivine in the Udachnaya-East kimberlite (Yakutia, Russia): types, compositions and origins. *J. Petrol.* **49**(4), 823–839.

Kelley S. P. and Wartho J. A. (2000) Rapid kimberlite ascent and the significance of Ar-Ar ages in xenolith phlogopites. *Science* **289**(5479), 609–611.

Lim E., Giuliani A., Phillips D. and Goemann K. (2018) Origin of complex zoning in olivine from diverse, diamondiferous kimberlites and tectonic settings: Ekati (Canada), Alto Paranaiba (Brazil) and Kaalvallei (South Africa). *Mineral. Petrol.*, 1–16.

Lynn K. J., Shea T., Garcia M. O., Costa F. and Norman M. D. (2018) Lithium diffusion in olivine records magmatic priming of explosive basaltic eruptions. *Earth Planet. Sci. Lett.* **500**, 127–135.

Mallmann G., O'Neill H. S. C. and Klemme S. (2009) Heterogeneous distribution of phosphorus in olivine from otherwise well-equilibrated spinel peridotite xenoliths and its implications for the mantle geochemistry of lithium. *Contrib. Miner. Petrol.* **158**(4), 485–504.

Manzini M., Bouvier A. S., Baumgartner L. P., Müntener O., Rose-Koga E. F., Schiano P. and Shimizu N. (2017) Weekly to monthly time scale of melt inclusion entrapment prior to eruption recorded by phosphorus distribution in olivine from mid-ocean ridges. *Geology* **45**(12), 1059–1062.

McCanta M. C., Beckett J. R. and Stolper E. M. (2016) Correlations and zoning patterns of phosphorus and chromium in olivine from H chondrites and the LL chondrite Semarkona. *Meteorit. Planet. Sci.* **51**(3), 520–546.

Milman-Barris M. S., Beckett J. R., Baker M. B., Hofmann A. E., Morgan Z., Crowley M. R. and Stolper E. (2008) Zoning of phosphorus in igneous olivine. *Contrib. Miner. Petrol.* **155**(6), 739–765.

Mitchell R. H. (2008) Petrology of hypabyssal kimberlites: relevance to primary magma compositions. *J. Volcanol. Geoth. Res.* **174**(1–3), 1–8.

Mitchell R. H. (1986) *Kimberlites. Mineralogy, Geochemistry, and Petrology*. Plenum Press, New York and London.

Moore A. E. (2017) Quantitative modelling of the apparent decoupling of Mg# and Ni in kimberlitic olivine margins: comment on Cordier et al.(Journal of Petrology, 56, 1775–1796, 2015). *J. Petrol.* **58**(2), 385–390.

Moore A. and Costin G. (2016) Kimberlitic olivines derived from the Cr-poor and Cr-rich megacryst suites. *Lithos* **258**, 215–227.

Nowell G. M., Pearson D. G., Bell D. R., Carlson R. W., Smith C. B., Kempton P. D. and Noble S. R. (2004) Hf isotope systematics of kimberlites and their megacrysts: new constraints on their source regions. *J. Petrol.* **45**(8), 1583–1612.

Peslier A. H., Woodland A. B. and Wolff J. A. (2008) Fast kimberlite ascent rates estimated from hydrogen diffusion profiles in xenolithic mantle olivines from southern Africa. *Geochim. Cosmochim. Acta* **72**(11), 2711–2722.

Pilbeam L. H., Nielsen T. F. D. and Waight T. E. (2013) Digestion fractional crystallization (DFC): an important process in the genesis of kimberlites. Evidence from olivine in the Majuagaa kimberlite, southern West Greenland. *J. Petrol.* **54**(7), 1399–1425.

Reitano R., Smith P. M. and Aziz M. J. (1994) Solute trapping of group III, IV, and V elements in silicon by an aperiodic stepwise growth mechanism. *J. Appl. Phys.* **76**(3), 1518–1529.

Roeder P. L. and Emslie R. (1970) Olivine-liquid equilibrium. *Contrib. Miner. Petrol.* **29**(4), 275–289.

Russell J. K., Porritt L. A., Lavallée Y. and Dingwell D. B. (2012) Kimberlite ascent by assimilation-fuelled buoyancy. *Nature* **481** (7381), 352.

Tschegg C., Ntaflos T., Kiraly F. and Harangi S. (2010) High temperature corrosion of oolivine phenocrysts in Pliocene basalts from Banat, Romania. *Austrian J. Earth Sci.* **103**(1).

Sakyi P. A., Tanaka R., Kobayashi K. and Nakamura E. (2012) Inherited Pb isotopic records in olivine antecryst-hosted melt inclusions from Hawaiian lavas. *Geochim. Cosmochim. Acta* **95**, 169–195.

Shea T., Lynn K. J. and Garcia M. O. (2015) Cracking the olivine zoning code: Distinguishing between crystal growth and diffusion. *Geology* **43**(10), 935–938.

Shearer C. K., Aaron P. M., Burger P. V., Guan Y., Bell A. S. and Papike J. J. (2013) Petrogenetic linkages among fO2, isotopic enrichments-depletions and crystallization history in Martian basalts. Evidence from the distribution of phosphorus in olivine megacrysts. *Geochim. Cosmochim. Acta* **120**, 17–38.

Skinner E. M. W. (2008) The emplacement of class 1 kimberlites. *J. Volcanol. Geoth. Res.* **174**(1–3), 40–48.

Sobolev N. V., Sobolev A. V., Tomilenko A. A., Kuz'min D. V., Grakhanov S. A., Batanova V. G., Logvinova A. M., Bul'bak T. A., Kostrovitskii S. I., Yakovlev D. A. and Fedorova E. N. (2018) Prospects of search for diamondiferous kimberlites in the northeastern Siberian Platform. *Russ. Geol. Geophys.* **59**(10), 1365–1379.

Sobolev N. V., Sobolev A. V., Tomilenko A. A., Kovyazin S. V., Batanova V. G. and Kuz'min D. V. (2015) Paragenesis and complex zoning of olivine macrocrysts from unaltered kimberlite of the Udachnaya-East pipe, Yakutia: relationship with the kimberlite formation conditions and evolution. *Russ. Geol. Geophys.* **56**(1–2), 260–279.

Sobolev A. V., Hofmann A. W., Kuzmin D. V., Yaxley G. M., Arndt N. T., Chung S. L. and Gurenko A. A. (2007) The amount of recycled crust in sources of mantle-derived melts. *Science* **316**(5823), 412–417.

Soltys A., Giuliani A. and Phillips D. (2018) A new approach to reconstructing the composition and evolution of kimberlite melts: a case study of the archetypal Bultfontein kimberlite (Kimberley, South Africa). *Lithos* **304**, 1–15.

Streck M. J. (2008) Mineral textures and zoning as evidence for open system processes. *Rev. Mineral. Geochem.* **69**(1), 595–622.

Watson E. B., Cherniak D. J. and Holycross M. E. (2015) Diffusion of phosphorus in olivine and molten basalt. *Am. Mineral.* **100** (10), 2053–2065.

Welsch B., Hammer J. and Hellebrand E. (2014) Phosphorus zoning reveals dendritic architecture of olivine. *Geology* **42**(10), 867–870.

Xing C. M., Wang C. Y. and Tan W. (2017) Disequilibrium growth of olivine in mafic magmas revealed by phosphorus zoning patterns of olivine from mafic–ultramafic intrusions. *Earth Planet. Sci. Lett.* **479**, 108–119.

Associate editor: James M.D. Day